Spin gap in the weakly interacting quantum spin chain antiferromagnet $KCuPO_4 \cdot H_2O$

M. Fujihala [1,2,*] M. Hagihala,[3] K. Morita,[4] N. Murai,[5] A. Koda,[6] H. Okabe,[6,7] and S. Mitsuda[2]

[1]*Advanced Science Research Center, Japan Atomic Energy Agency, Tokai-mura, Ibaraki 319-1195, Japan*
[2]*Department of Physics, Faculty of Science, Tokyo University of Science, Shinjuku, Tokyo 162-8601, Japan*
[3]*Materials Sciences Research Center, Japan Atomic Energy Agency, Tokai, Ibaraki 319-1195, Japan*
[4]*Department of Physics, Faculty of Science and Technology, Tokyo University of Science, Chiba 278-8510, Japan*
[5]*J-PARC Center, Japan Atomic Energy Agency, Tokai, Ibaraki 319-1195, Japan*
[6]*Muon Science Laboratory and Condensed Matter Research Center, Institute of Materials Structure Science,*
High Energy Accelerator Research Organisation, 1-1 Oho, Tsukuba 305-0801, Japan
[7]*Institute for Materials Research, Tohoku University (IMR), 2-1-1 Katahira, Aoba-ku, Sendai 980-8577, Japan*

The $S = 1/2$ Heisenberg linear chain antiferromagnet is the simplest spin model; nevertheless it serves as a platform for various quantum many-body phenomena. Here, we report the magnetic behavior of a quasi-one-dimensional antiferromagnet $KCuPO_4 \cdot H_2O$. A long-range commensurate antiferromagnetic order with ordered moment 0.31(1) μ_B per spin occurs at $T_N = 11.7(1)$ K. Above T_N, the inelastic neutron excitation is characterized by a two spinon continuum. The intrachain interaction J and interchain interaction $|J'|$ are estimated to be 172 and 4.25(4) K, respectively; thus the ratio of $|J'|/J = 0.0247(3)$. At lower energies, below T_N, a spin gap is observed in the dispersive excitations. These results are consistent with characteristics observed in a weakly interacting $S = 1/2$ Heisenberg chain system.

I. INTRODUCTION

Low-dimensional spin systems are expected to be promising candidates for novel quantum states. The simplest one-dimensional (1D) system is a linear chain model as follows:

$$\mathcal{H} = J \sum_{\langle i \rangle} \boldsymbol{S}_i \cdot \boldsymbol{S}_{i+1}, \tag{1}$$

where J represents nearest neighbor magnetic coupling. In case J is antiferromagnetic, i.e., $J > 0$, the ground state is a gapless quantum spin liquid in which spin-spin correlation decays algebraically with distance. In real $S = 1/2$ linear chain magnets, often long-range magnetic order at finite temperatures is induced by weak interchain coupling. However, a dimensional crossover behavior can be observed in a weakly interacting quantum spin chain antiferromagnet, which is the $S = 1/2$ Heisenberg linear chain antiferromagnet with relatively weak interchain interactions [1,2]. In the system, below the Néel temperature T_N, single magnon excitations are observed at lower energies and multimagnon continuum excitations are observed at higher energies in the inelastic neutron-scattering (INS) spectrum. The excitation at lower energies is characterized by the presence of a longitudinal mode. The longitudinal mode was observed in $KCuF_3$ [3–5], confirming theoretical predictions based on chain-mean-field (chain-MF) [6] and random-phase approximation (RPA) [1,2] theories. However, the chain-MF/RPA cannot explain the experimentally observed finite lifetime of the longitudinal

mode of $KCuF_3$. In another model compound $BaCu_2Si_2O_7$, the transverse-polarized INS spectrum is in excellent agreement with chain-MF/RPA theory [7–11]. At the 1D Brillouin zone centers, the excitation is separated from the single magnon modes by an energy gap. In contrast, the longitudinal-polarized spectrum of $BaCu_2Si_2O_7$ is not consistent with this theory. It is concluded that this discrepancy is due to the intrinsic limitations of the RPA that ignore correlation effects. The primary difference between the two compounds is the magnitude of the interchain interaction J'. In $BaCu_2Si_2O_7$, the ratio of $J'/J \approx 0.01$ [8], whereas it is approximately 0.04 for $KCuF_3$ [12,13]. Further studies using a new model compound with the ratio of $0.01 < J'/J < 0.04$ lead to a deeper understanding of the spin states in this system, particularly, the factors that stabilize the longitudinal mode. Here we report magnetic behaviors of $KCuPO_4 \cdot H_2O$ which is a new weakly interacting quantum spin chain antiferromagnet. We investigated the magnetism in this compound through magnetic susceptibility, muon-spin rotation and relaxation (μSR), neutron powder diffraction (NPD), and INS measurements.

II. EXPERIMENTAL AND COMPUTATIONAL DETAILS

Polycrystalline $KCuPO_4 \cdot H_2O$ was prepared using a solution reaction [14]. Aqueous solutions of 0.2-M $CuSO_4$ and 1.8-M K_2HPO_4 were mixed and stirred at 90 °C for 24 h. The product was then thoroughly washed with pure water. The deuterated samples were produced for the neutron-scattering experiments. NPD measurements were performed on a deuterated sample using a SuperHRPD time-of-flight diffractometer with a highest resolution of $\Delta d/d = 0.035\%$ installed at the Material and Life Science Facility (MLF) at Japan Proton
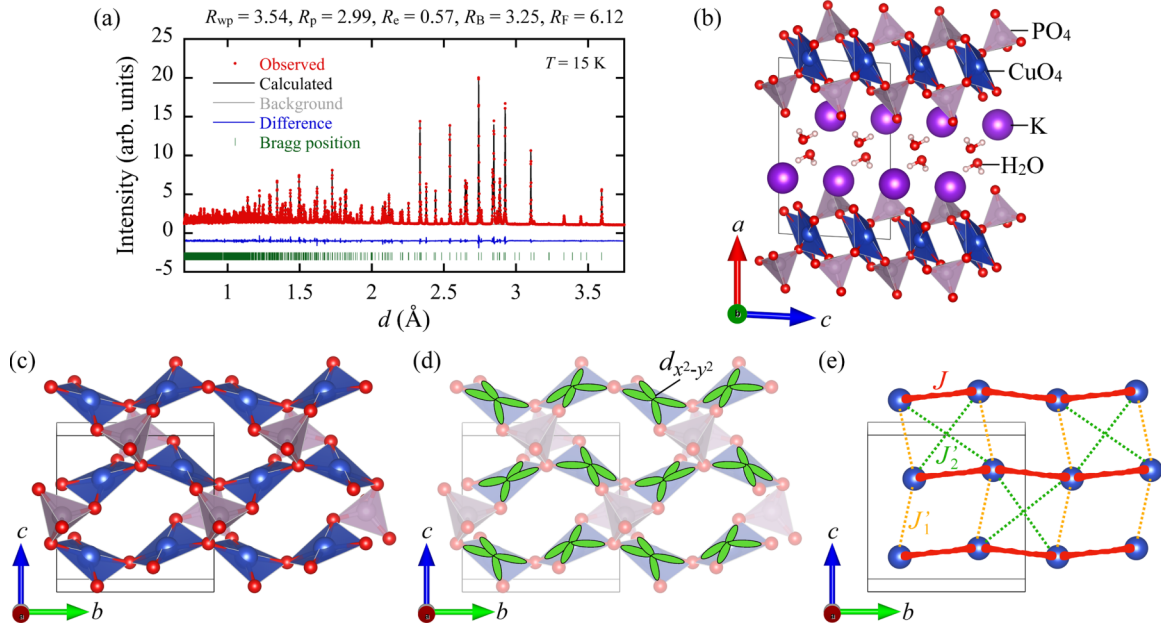
*fujihala@post.j-parc.jp

FIG. 1. (a) NPD intensity pattern (filled red circles) observed for $KCuPO_4 \cdot D_2O$ at 15 K, the result of Rietveld refinement using the computer program RIETAN-FP (black solid line), and the difference between the calculated and observed intensities (blue solid line). The green vertical bars indicate the position of Bragg reflection peaks. (b) Crystal structure of $KCuPO_4 \cdot H_2O$. The Cu^{2+} ions (blue) and K^+ ions (purple) displayed with nearby H_2O and PO_4. The Cu^{2+} ions have tetracoordination. (c) Chains of CuO_4 plaquettes are stringed up along the b axis. (d) Schematic of the arrangement of Cu^{2+} orbitals for $KCuPO_4 \cdot H_2O$. $d_{x^2-y^2}$ orbitals carrying spin 1/2 are depicted on Cu sites. (e) Effective spin model of $KCuPO_4 \cdot H_2O$ with the intrachain interaction J, and the interchain interactions J_1' and J_2'.

Accelerator Research Complex (J-PARC) [15,16]. The crystal structure of $KCuPO_4 \cdot H_2O$ was refined by Rietveld analysis with Z-RIETVELD software, using high-resolution NPD profiles obtained from the backscattering (BS) bank [17,18]. The magnetic structure was refined by Rietveld analysis with Z-RIETVELD and FULLPROF software, using the high-resolution NPD profiles obtained from the BS bank, 90° (QA) bank, and low-angle (LA) bank, respectively [17–19]. Magnetic susceptibility measurements were performed using a commercial superconducting quantum interference device magnetometer (Quantum Design). The μSR experiments were performed using the spin-polarized pulsed surface-muon (μ^+) beam at the S1 beamline of the MLF at J-PARC. The spectra were collected in the temperature range from 4.6 to 300 K using a ^{4}He cryostat. The INS spectra in a wide momentum-energy range were measured using the cold-neutron disk chopper spectrometer AMATERAS installed in the MLF at J-PARC [20]. The sample was cooled to 4 K using a bottom-loading closed cycle refrigerator. We optimized the chopper condition to yield incident neutron energies of $E_i = 42.04$, 15.16, 7.74, and 1.48 meV, with corresponding energy resolutions at the elastic line of $\Delta E = 2.64$, 0.69, 0.20, and 0.022 meV, respectively (full width at half maximum). Data reduction and analysis were performed using the UTSUSEMI software package [21]. Magnetic susceptibility of $KCuPO_4 \cdot H_2O$ is calculated by the finite temperature Lanczos (FTL) method for 30 sites [22].

III. RESULTS AND DISCUSSION

Figure 1(a) depicts NPD patterns for deuterated sample $KCuPO_4 \cdot D_2O$ collected at 15 K, and the results of

Rietveld refinement. The analysis was based on the monoclinic $P2_1/c$ structure reported by Laügt and Tordjman [14]. The lattice parameters are refined as $a = 10.487\,536(4)$ Å, $b = 6.784\,207(3)$ Å, $c = 6.678\,871(3)$ Å, and $\beta = 93.313\,77(4)°$, and the positions of the individual atoms are also determined as presented in Table I. These results are consistent with those of previous report [14]. About 30% of D_2O in this compound was replaced by H_2O, probably caused

TABLE I. Structure information of $KCuPO_4 \cdot H_2O$ refined from NPD data measured at 15 K.

Chemical formula		$KCuPO_4 \cdot H_2O$		
Cell setting		Monoclinic		
Space group		$P2_1/c$		
a (Å)		10.487536(4)		
b (Å)		6.784207(3)		
c (Å)		6.678871(3)		
β (°)		93.31377(4)		
Atom	x	y	z	g
K	0.31468(3)	0.57571(5)	0.53967(6)	1
Cu	−0.006462(19)	0.20384(2)	0.22117(3)	1
P	0.17693(2)	0.46733(4)	−0.00025(4)	1
O1	0.31368(2)	0.46751(3)	−0.05957(3)	1
O2	0.16219(2)	0.61435(3)	0.17326(4)	1
O3	0.08337(2)	0.53547(4)	−0.18356(3)	1
O4	0.13008(2)	0.25847(3)	0.04998(4)	1
D1	0.41578(5)	0.38391(6)	0.16327(7)	0.6815(5)
H1	0.41578(5)	0.38391(6)	0.16327(7)	0.3185(5)
D2	0.40100(4)	0.22066(6)	0.33108(6)	0.7235(6)
H2	0.40100(4)	0.22066(6)	0.33108(6)	0.2765(6)

by using H_2O when the sample was washed. As shown in Fig. 1(b), the D_2O exists only between the potassium layers. The copper ions are not coordinated with the oxygen ions of D_2O; thus, it is unlikely that the D_2O/H_2O replacement will affect the magnetism of $KCuPO_4 \cdot D_2O$. The chains of CuO_4 plaquettes are strung up along the b axis [Fig. 1(c)]. The orbital arrangements can be deduced reasonably from the positions of oxygen around the Cu^{2+} ion. According to crystal field theory, the five $3d$ orbitals in a square-planar field are produced by four surrounding anions split into e_g, a_{1g}, b_{2g}, and b_{1g} orbitals with different energies. Since the b_{1g} orbital possesses the highest energy, all the Cu^{2+} ions have their unpaired electrons in the $d_{x^2-y^2}$ orbital [Fig. 1(d)]. The Cu-O-Cu angle significantly influences the value of the exchange interactions [23]. The nearest-neighbor magnetic coupling J is the superexchange interaction through the Cu-O3-Cu bond with a bond angle of $120.24°$ in Fig. 1(e). J is expected to be the strong antiferromagnetic interaction (see, for example, Fig. 1 in Ref. [24]). Furthermore, the exchange interactions through the Cu-O-P-O-Cu exchange paths are denoted by J'_1 and J'_2. When both J'_1 and J'_2 are strong, namely J'_1 and $J'_2 \sim J$, the effective spin model of $KCuPO_4 \cdot H_2O$ can be regarded as a distorted checkerboard lattice, whereas in the case that they are weak, the compound can be regarded as weakly interacting quantum spin chains. The system exhibits the magnetic behavior of weakly interacting quantum spin chains, as discussed below.

Figure 2 presents the temperature dependence of the magnetic susceptibility χ and the inverse magnetic susceptibility $1/\chi$ of $KCuPO_4 \cdot H_2O$ in the temperature range 1.8–300 K. The temperature dependences of the magnetic susceptibilities of $KCuPO_4 \cdot D_2O$ and $KCuPO_4 \cdot H_2O$ are in good agreement (see Supplemental Material for details [25]). Thus, we conclude that the D_2O/H_2O replacement has no significant effect on intrachain and interchain interactions. The χ is obtained by subtracting Pascal's diamagnetic contribution from the experimental data [26]. The temperature dependence of χ is the maximum around $T = 150$ K and has a peak at $T_N = 11.7(1)$ K, as shown in Fig. 2(a) and the inset. We estimated the Curie constant and Curie-Weiss temperature from $1/\chi$ with the Curie-Weiss law $C/(T - \theta_{CW})$, between 250 and 300 K as $C = 0.52(5)$ emu K/mol-Cu and $\theta_{CW} = -218(4)$ K, respectively. C corresponds to an effective moment of $2.04(4)$ μ_B, which is slightly higher than the spin-only value (= 1.73 μ_B). In order to estimate the magnitude of the exchange interactions, we calculated the χ by FTL method [22]. As shown in Fig. 2(b), we succeeded in reproducing the χ curve of $KCuPO_4 \cdot H_2O$ with the $S = 1/2$ Heisenberg linear chain model with $J = 172$ K and $g = 2.11$, where g is the gyromagnetic ratio. The magnitudes of J'_1 and J'_2 are difficult to determine from the only χ data. In addition, the formation of the long-range magnetic order indicates the existence of an interchain interaction J'_a along the a axis. However, they should be much smaller than J, because of good agreement between the experimental data and the FTL calculation. In the weakly interacting quantum spin chain system, the interchain interaction $|J'|$ can be estimated using the predictions of the chain-MF model [1]. We estimated the $|J'| = 4.25(4)$ K of $KCuPO_4 \cdot H_2O$, and thus the ratio of $|J'|/J = 0.0247(3)$. This value of $|J'|/J$ indicates that $KCuPO_4 \cdot H_2O$ has "moderately
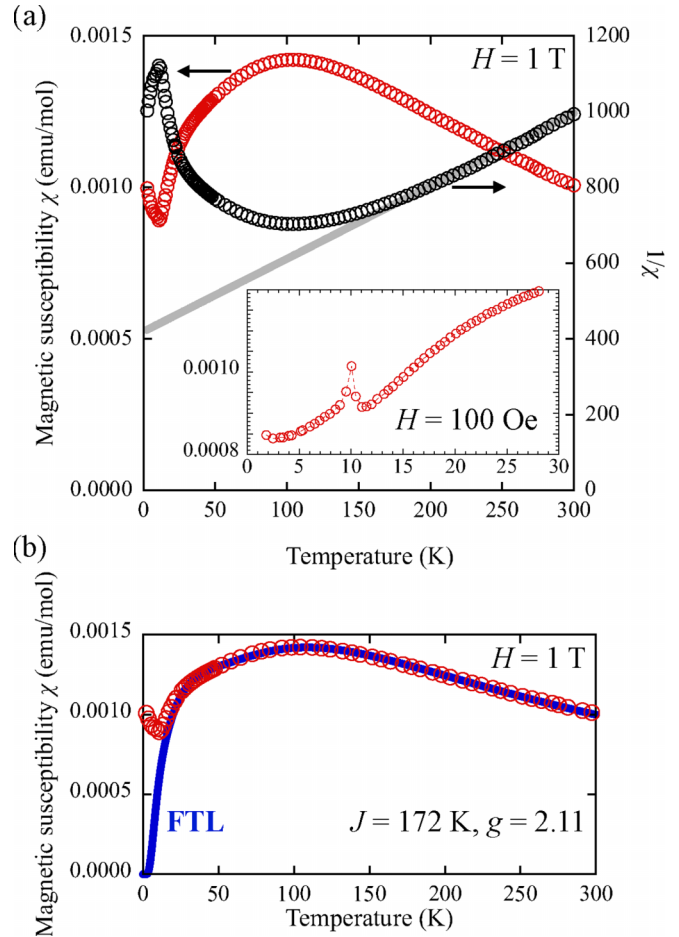

FIG. 2. (a) Temperature dependence of magnetic susceptibility χ (open red circles, left axis) and their inverse susceptibility $1/\chi$ (open black circles, right axis) measured at 1 T. The straight line obeys the Curie-Weiss law. The inset plot depicts the susceptibilities measured at 100 Oe. (b) Temperature dependence of χ and the fitted calculation data obtained by the FTL method for 30 sites.

weak interchain interactions" suitable for investigation of a dimensional crossover phenomenon.

Zero-field (ZF)-μSR measurements provide evidence for static magnetic ordering in $KCuPO_4 \cdot H_2O$. The muon spin precession frequencies are observed and disappear at $T_N = 11.7(1)$ K, as shown in Fig. 3(a). The spectra for $T < T_N$ are best fit by

$$A_0 P_{ZF}(t) = A_1 \left(\frac{1}{3} \exp(-\lambda_1 t) + \frac{2}{3} \exp(-\lambda_2 t) \cos(\gamma_\mu B_1 t) \right)$$
$$A_2 \left(\frac{1}{3} \exp(-\lambda_3 t) + \frac{2}{3} \exp(-\lambda_4 t) \cos(\gamma_\mu B_2 t) \right)$$
$$+ A_{BG}, \tag{2}$$

where A_0 is the initial asymmetry, A_1 and A_2 are the intrinsic asymmetries $A_1 = 0.127$ and $A_2 = 0.077$, A_1 represents the fraction of muons that stop near H_2O, and A_2 represents the fraction of muons that stop at different muon sites. A_{BG} is the constant background $A_{BG} = 0.0112$. λ_i ($i = 1$–4) are the relaxation rates of the transverse and longitudinal components, respectively, and B_j ($j = 1$ and 2) are internal magnetic
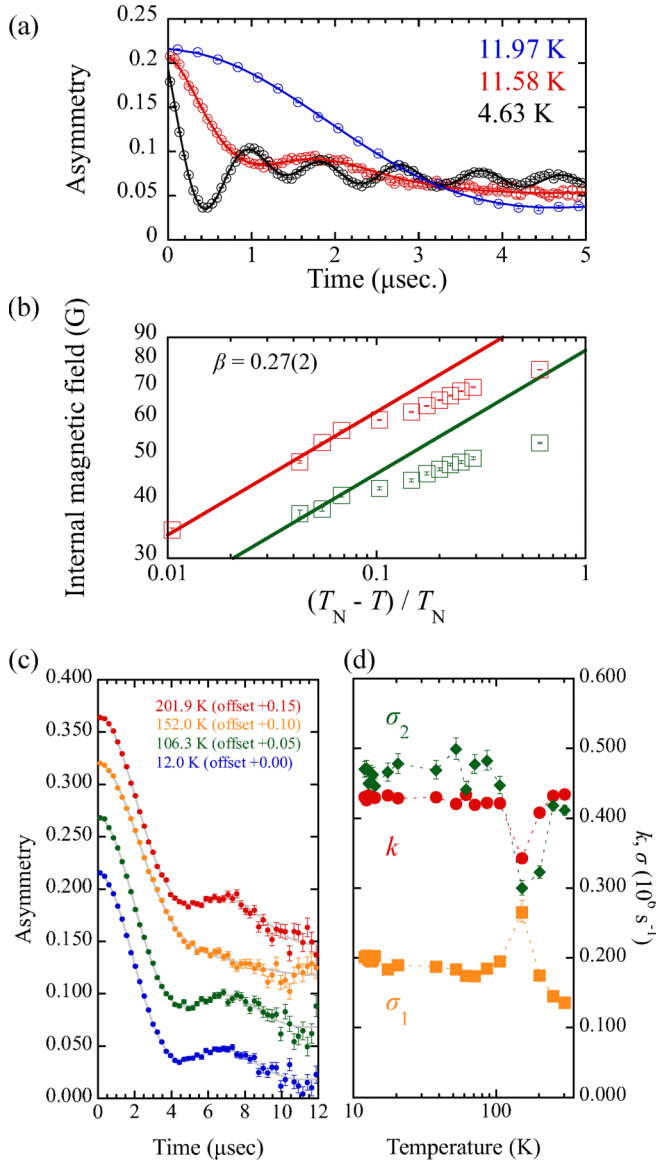
FIG. 3. (a) ZF-μSR spectra at representative temperatures. The thick lines behind the data points are the fitted curves (see text for details). (b) Temperature dependence of the internal magnetic fields for KCuPO$_4 \cdot$ H$_2$O. The dashed lines show power-law fits. (c) ZF-μSR spectra measured above T_N, showing the fitted time window up to 12 μs. (d) Temperature dependence of relaxation rate σ_1, σ_2, and k (see text for details).

fields. For $T > T_N$, the spectra are well fitted by

$$
A_0 P_{ZF}(t) = A_1 G^{tri}(t) \exp\left(-\frac{\sigma_1^2 t^2}{2}\right)
$$
$$
+ A_2 \exp\left(-\frac{\sigma_2^2 t^2}{2}\right) + A_{BG}, \quad (3)
$$

where σ_1 and σ_2 are the Gaussian relaxation rates; $G^{tri}(t)$ is the muon spin depolarization function caused by forming a three spin-one-half system. The $G^{tri}(t)$ signal is represented

by [27]

$$
G^{tri}(t) = 0.285\,70 + 0.234\,29 \cos(1.920\,58kt)
$$
$$
+ 0.137\,19 \cos(1.753\,41kt)
$$
$$
+ 0.051\,69 \cos(1.151\,84kt)
$$
$$
+ 0.027\,50 \cos(0.768\,74kt)
$$
$$
+ 0.186\,97 \cos(0.601\,56kt)
$$
$$
+ 0.076\,55 \cos(0.167\,18kt), \quad (4)
$$

where

$$
k = (\sqrt{2}/d_{H-\mu})^3. \quad (5)
$$

$d_{H-\mu}$ represents the distance between H and μ, namely the length of the edge of the equilateral triangle formed by two H and one μ. The first term in Eq. (2), which multiplies $G^{tri}(t)$ by a Gaussian function, is a phenomenological approach that considers the effects of next-nearest-neighbor hydrogen ions, etc.

The temperature dependence of the internal magnetic fields decreases with increasing temperature and vanishes at T_N. Analyzing the data with the power law,

$$
B_j = B_j(0)[1 - (T/T_N)]^\beta, \quad (6)
$$

yields the critical exponent $\beta = 0.27(2)$, and the internal magnetic fields $B_1(0) = 114.6$ G and $B_2(0) = 84.3$ G [Fig. 3(b)]. The value of β is below the critical exponent for a three-dimensional magnetic system ($\beta = 0.36$) and is in good agreement with the critical exponent measured in the BaCu$_2$Si$_2$O$_7$ [$\beta = 0.25(5)$] [8].

As shown in Fig. 3(c), the spectra observed at 201.9 and 12.0 K show almost the same shape. In fact, there is no significant difference in the fitting parameters [Fig. 3(d)]. The changes in the spectra observed above T_N are only observed around 152 K. The spectrum at 152 K can be interpreted as some changes in the crystal lattice. Excluding the data around 152K, the average value of k is 0.427(5); thus, $d_{H-\mu}$ is estimated as 1.88(1) Å. The value of $d_{H-\mu}$ is consistent with the length of the edge of the equilateral triangle of the H ions in the oxonium ion.

The lattice constants and atomic positions are refined in the same space group at all temperature regions. As shown in Figs. 4(a)–4(d), no significant changes in the lattice parameters are observed. However, the Cu-O-Cu bond angle increases up to around 150 K and does not change below that temperature, indicating a temperature dependency distinct from the lattice parameters. The Cu-O-P-O-Cu bond angle should also change when the Cu-O-Cu bond angle is changed. These results suggest that the copper and phosphate ions change their positions to stabilize the one-dimensionality of this system by enhancing the magnetic interaction J while simultaneously weakening J_1' and J_2'. This change has been observed using different measurement methods, including magnetic susceptibility, μSR, and NPD.

To determine the magnetic structure, we performed neutron diffraction measurements below T_N. As shown in Figs. 5(a)–5(c), at least four peaks are found at 4 K that do not appear above T_N. These peaks can be indexed with the propagation vector $\mathbf{k} = (\frac{1}{2}, 0, 0)$. As shown in Fig. 5(d), a candidate
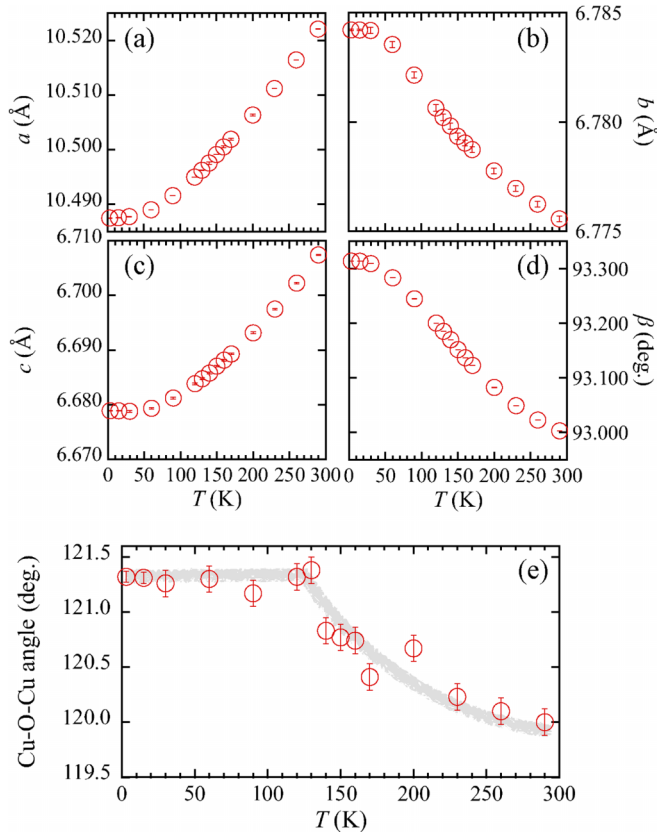
FIG. 4. (a–d) Temperature dependence of the lattice parameters a, b, c, and β. (e) Temperature dependence of the bond angle of Cu-O3-Cu.

magnetic structure is obtained. The magnetic structure of $KCuPO_4 \cdot D_2O$ is a simple Néel-type order along the chain. The spins point along the a axis, although it is difficult to determine the deviation of the spins from the a axis based on these data. However, at least, we reveal that an incommensurate magnetic structure is not formed in $KCuPO_4 \cdot D_2O$. The magnitude of the magnetic moment is estimated as $m = 0.31(1)\,\mu_B$, which is smaller than that of $KCuF_3$ and larger than that of $BaCu_2Si_2O_7$ [8,13].

Figure 6 shows the magnitude of the magnetic moment for the known weakly interacting quantum spin chain antiferromagnets as a function of $|J'|/J$ [8]. Both the magnitude of the magnetic moment and the ratio of $|J'|/J$ of $KCuPO_4 \cdot H_2O$ are located between $KCuF_3$ and $BaCu_2Si_2O_7$, indicating that this compound has moderately weak interchain interactions. Furthermore, the relationship between these values appears to be in good agreement with the predictions of the chain-MF model.

The INS experiments are performed on a powder sample of $KCuPO_4 \cdot D_2O$. In a powder sample of an ideal $S = 1/2$ Heisenberg linear chain antiferromagnet, gapless excitation from the Brillouin zone center at $Q = \frac{\pi}{d}$ (d is the distance between neighboring spins), van Hove singularity at the spinon continuum edge, and magnetic excitations tailing toward the high Q side are all observed in the INS spectrum (see, for example, Refs. [28,29]). To confirm these features, the lower and upper energy boundaries of the spinon continuum of the
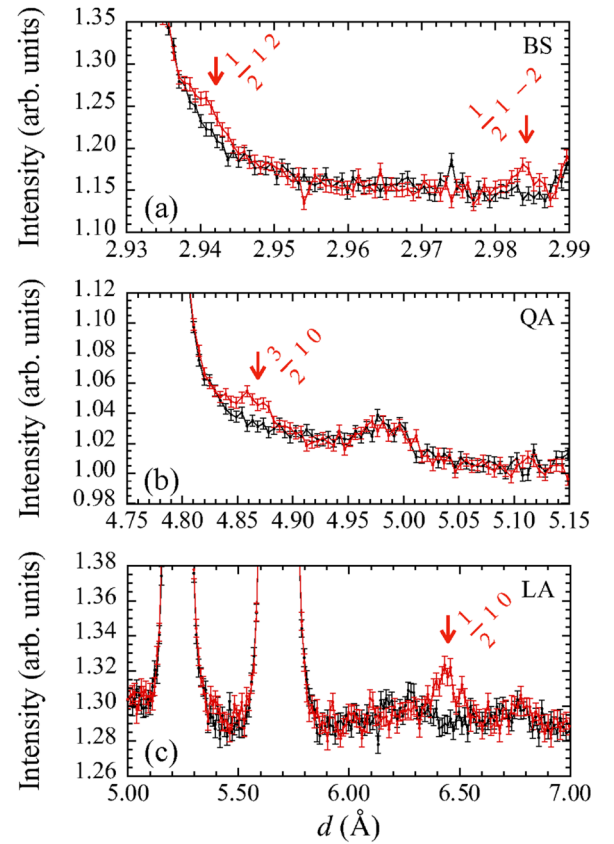

FIG. 5. NPD patterns measured at 3 K (filled red circles) and 15 K (filled black circles) focused on the magnetic reflections. The data are collected by (a) BS, (b) QA, and (c) LA banks. (d) Possible magnetic structure of $KCuPO_4 \cdot H_2O$.

linear chain given by $(\pi J/2)|\sin(Qd)|$ and $\pi J|\sin(Qd/2)|$ are shown in the spectra [4,30]. Here, $J = 172$ K and $d = b/2$, where b is the lattice constant. As shown in Fig. 7(a), similar magnetic excitations are observed above and below T_N. It is evident that the excitation rises from the Brillouin zone center along the chain direction, $Q = \frac{\pi}{b/2} \approx 0.93\ Å^{-1}$. Figure 7(b)
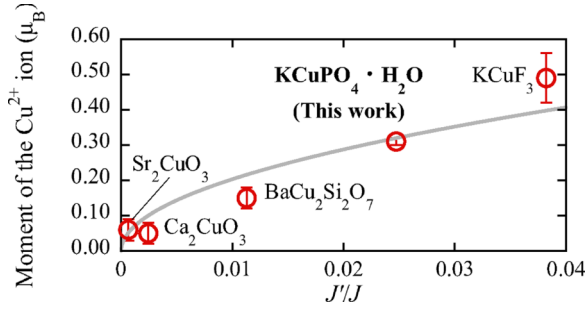
FIG. 6. The magnitude of the magnetic moment for the known weakly interacting quantum spin chain antiferromagnets as a function of $|J'|/J$. The $|J'|$ for $KCuPO_4 \cdot H_2O$ is estimated from the predictions of the chain-MF model [1]. See Fig. 1 in Ref. [8] for detailed information on other magnets. The lines are predictions of the chain-MF model [1].

shows the INS spectrum in a wide energy range, indicating that phonon excitations are dominant at high energies. However, a comparison of the 100-K data corrected for the phonon population factor with the 15-K data confirms the presence of a magnetic signal. The Q dependence of the INS intensity after integration over a finite energy interval is shown in Fig. 7(c). The peak around the Brillouin zone center is observed on the low-energy side. Furthermore, the flat signal is observed around the spinon continuum edge on the high-energy side. The signal due to magnetic excitation is generally enhanced at low Q values, whereas phonon excitation is dominant at high Q values. The intensity at 23 meV seems to increase

with decreasing Q, indicating that it comes from magnetic excitation. Therefore, the spectrum measured at 15 K is confirmed to have the characteristics of magnetic excitation of the $S = 1/2$ Heisenberg linear chain antiferromagnet. As shown in Figs. 7(d) and 7(e), the spin gap opens below T_N. The incommensurability shifts from the Brillouin zone center are not seen in the spectrum. The gap energy $\Delta \approx 0.7 = 1.9|J'|$ is in good agreement with the chain-MF/RPA theory [11]. As shown in Fig. 7(f), the INS intensity remains even below $E = 0.7$, suggesting the existence of of components with different gap sizes, i.e., longitudinal and transverse modes. In addition, at 4 K, the Q dependence of INS intensity after integration at $4.0 < E < 5.0$ meV increases around the spinon continuum edge, while the intensity slightly decreases in the region within the boundaries [Fig. 7(g)]. This indicates that the single magnon excitations are observed at lower energies.

IV. CONCLUSIONS

In summary, we presented $KCuPO_4 \cdot H_2O$ as an ideal weakly interacting quantum spin chain antiferromagnet. One-dimensional short-range correlations are developed below 150 K, and a Néel-type antiferromagnetic order is formed at $T_N = 11.7(1)$ K. The estimated ordered magnetic moment is small, about $0.31(1)$ μ_B, indicating that the quantum effect suppresses the moment. The excitation spectra exhibit the features of the $S = 1/2$ Heisenberg linear chain antiferromagnet. Below T_N, we observed the spin gap and other features peculiar to the weakly interacting quantum spin chains.
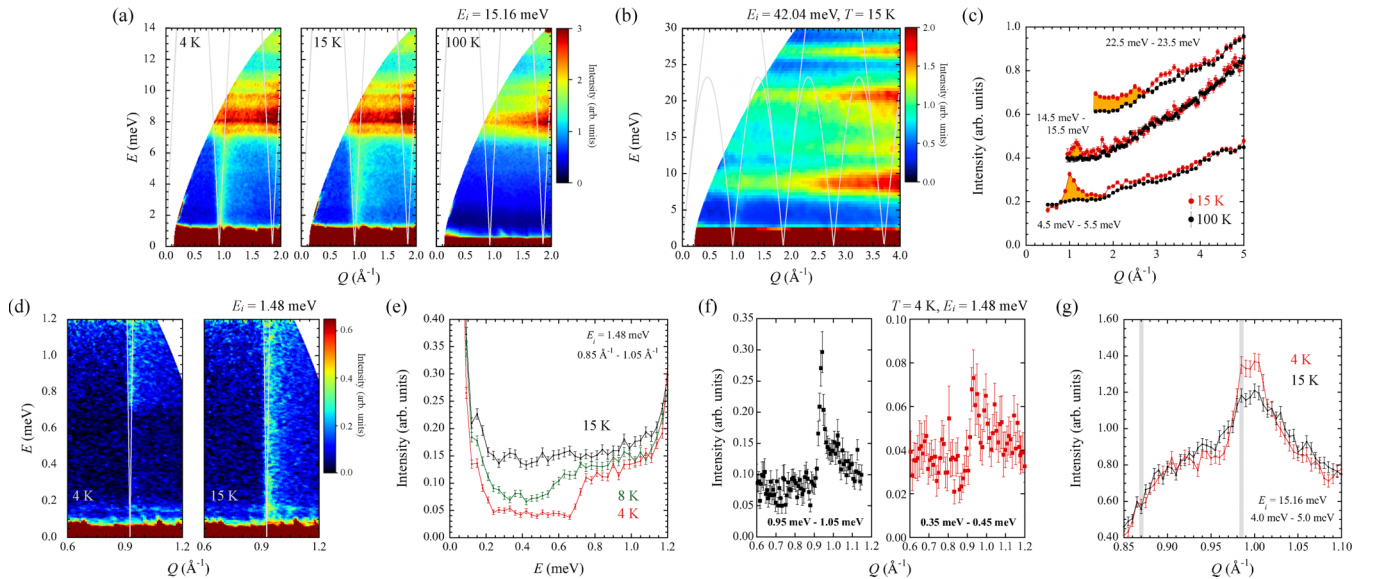

FIG. 7. (a) INS spectra at 4 K (left), 15 K (center), and 100 K (right) were observed with an incident neutron energy of 15.16 meV. The superimposed gray solid lines indicate the lower and upper energy boundaries of the continuum (see text for details). (b) INS spectra at 15 K were observed with an incident neutron energy of 42.04 meV. (c) Q dependence of the scattering integrated over energy transfers $4.5 < E < 5.5$, $14.5 < E < 15.5$, and $22.5 < E < 23.5$ meV measured at 15 K (filled red circles) and 100 K (filled black circles). The colored areas indicate the magnetic excitation components. (d) INS spectra at 4 K (left) and 15 K (right) were observed with an incident neutron energy of 1.48 meV. (e) Energy dependence of the scattering integrated over Q in the range 0.85 Å^{-1} $< Q < 1.05$ mÅ^{-1}, measured at 4, 8, and 15 K. (f) Q dependence of the scattering integrated over energy transfers $0.95 < E < 1.05$ meV (left) and $0.35 < E < 0.45$ meV (right) measured at 4 K. (g) Q dependence of the scattering integrated over energy transfers $4.0 < E < 5.0$ meV measured at 4 K (filled red circles) and 15 K (filled black circles). The gray lines indicate the spinon continuum edge at $E = 4.5$ meV.

Our comprehensive experiments reveal that $KCuPO_4 \cdot H_2O$ is a good candidate for a weakly interacting quantum spin chain system next to $KCuF_3$ and $BaCu_2Si_2O_7$; however, a quantitative comparison of the experimental results with the chain-MF/RPA theory has not been achieved. Further studies with single-crystal neutron-scattering experiments will greatly advance our understanding of this system.

[1] H. J. Schulz, Dynamics of Coupled Quantum Spin Chains, Phys. Rev. Lett. **77**, 2790 (1996).

[2] F. H. L. Essler, A. M. Tsvelik, and G. Delfino, Quasi-one-dimensional spin-$\frac{1}{2}$ Heisenberg magnets in their ordered phase: Correlation functions, Phys. Rev. B **56**, 11001 (1997).

[3] B. Lake, D. A. Tennant, and S. E. Nagler, Novel Longitudinal Mode in the Coupled Quantum Chain Compound $KCuF_3$, Phys. Rev. Lett. **85**, 832 (2000).

[4] B. Lake, D. A. Tennant, C. D. Frost, and S. E. Nagler, Quantum criticality and universal scaling of a quantum antiferromagnet, Nat. Mater. **4**, 329 (2005).

[5] B. Lake, D. A. Tennant, and S. E. Nagler, Longitudinal magnetic dynamics and dimensional crossover in the quasi-one-dimensional spin-$\frac{1}{2}$ Heisenberg antiferromagnet $KCuF_3$, Phys. Rev. B **71**, 134412 (2005).

[6] D. J. Scalapino, Y. Imry, and P. Pincus, Generalized Ginzburg-Landau theory of pseudo-one-dimensional systems, Phys. Rev. B **11**, 2042 (1975).

[7] A. Zheludev, M. Kenzelmann, S. Raymond, E. Ressouche, T. Masuda, K. Kakurai, S. Maslov, I. Tsukada, K. Uchinokura, and A. Wildes, Energy Separation of Single-Particle and Continuum States in an $S = 1/2$ Weakly Coupled Chains Antiferromagnet, Phys. Rev. Lett. **85**, 4799 (2000).

[8] M. Kenzelmann, A. Zheludev, S. Raymond, E. Ressouche, T. Masuda, P. Böni, K. Kakurai, I. Tsukada, K. Uchinokura, and R. Coldea, Spin waves and magnetic ordering in the quasi-one-dimensional $S = \frac{1}{2}$ antiferromagnet $BaCu_2Si_2O_7$, Phys. Rev. B **64**, 054422 (2001).

[9] A. Zheludev, M. Kenzelmann, S. Raymond, T. Masuda, K. Uchinokura, and S.-H. Lee, Spin dynamics in the quasi-one-dimensional $S = \frac{1}{2}$ antiferromagnet $BaCu_2Si_2O_7$, Phys. Rev. B **65**, 014402 (2001).

[10] A. Zheludev, K. Kakurai, T. Masuda, K. Uchinokura, and K. Nakajima, Dominance of the Excitation Continuum in the Longitudinal Spectrum of Weakly Coupled Heisenberg $S = 1/2$ Chains, Phys. Rev. Lett. **89**, 197205 (2002).

[11] A. Zheludev, S. Raymond, L.-P. Regnault, F. H. L. Essler, K. Kakurai, T. Masuda, and K. Uchinokura, Polarization dependence of spin excitations in $BaCu_2Si_2O_7$, Phys. Rev. B **67**, 134406 (2003).

[12] S. K. Satija, J. D. Axe, G. Shirane, H. Yoshizawa, and K. Hirakawa, Neutron scattering study of spin waves in one-dimensional antiferromagnet $KCuF_3$, Phys. Rev. B **21**, 2001 (1980).

[13] M. T. Hutchings, E. J. Samuelsen, G. Shirane, and K. Hirakawa, Neutron-diffraction determination of the antiferromagnetic structure of $KCuF_3$, Phys. Rev. **188**, 919 (1969).

[14] M. B. Laügt and I. Tordjman, Structure cristalline de l'orthophosphate de cuivre-potassium monohydraté: $CuKPO_4 \cdot H_2O$, Acta Crystallogr. Sect. B **32**, 203 (1976).

[15] S. Torii, M. Yonemura, T. Y. S. P. Putra, J. R. Zhang, P. Miao, T. Muroya, R. Tomiyasu, T. Morishima, S. Sato, H. Sagehashi, Y. Noda, and T. Kamiyama, Super high resolution powder diffractometer at J-PARC, J. Phys. Soc. Jpn. **80**, SB020 (2011).

[16] S. Torii, M. Yonemura, Y. Ishikawa, P. Miao, R. Tomiyasu, S. Satoh, Y. Noda, and T. Kamiyama, Improvement of instrument devices for super high resolution powder diffractometer at J-PARC, J. Phys.: Conf. Ser. **502**, 012052 (2014).

[17] R. Oishi, M. Yonemura, Y. Nishimaki, S. Torii, A. Hoshikawa, T. Ishigaki, T. Morishima, K. Mori, and T. Kamiyama, Rietveld analysis software for J-PARC, Nucl. Instrum. Methods Phys. Res., Sect. A **600**, 94 (2009).

[18] R. Oishi-Tomiyasu, M. Yonemura, and T. Morishima, Application of matrix decomposition algorithms for singular matrices to the Pawley method in Z-Rietveld, J. Appl. Crystallogr. **45**, 299 (2012).

[19] J. Rodríguez-Carvajal, Recent advances in magnetic structure determination by neutron powder diffraction, Phys. B: Condens. Matter **192**, 55 (1993).

[20] K. Nakajima, S. Ohira-Kawamura, T. Kikuchi, M. Nakamura, R. Kajimoto, Y. Inamura, N. Takahashi, K. Aizawa, K. Suzuya, K. Shibata *et al.*, AMATERAS: A cold neutron disk chopper spectrometer, J. Phys. Soc. Jpn. **80**, SB028 (2011).

[21] Y. Inamura, T. Nakatani, J. Suzuki, and T. Otomo, Development status of software Utsusemi for chopper spectrometers at MLF, J-PARC, J. Phys. Soc. Jpn. **82**, SA031 (2013).

[22] J. Jaklič and P. Prelovsek, Lanczos method for the calculation of finite-temperature quantities in correlated systems, Phys. Rev. B **49**, 5065 (1994).

[23] Y. Mizuno, T. Tohyama, S. Maekawa, T. Osafune, N. Motoyama, H. Eisaki, and S. Uchida, Electronic states and magnetic properties of edge-sharing Cu-O chains, Phys. Rev. B **57**, 5326 (1998).

[24] T. Kimura, Y. Sekio, H. Nakamura, T. Siegrist, and A. P. Ramirez, Cupric oxide as an induced-multiferroic with high-T_C, Nat. Mater. **7**, 291 (2008).

[25] See Supplemental Material at http://link.aps.org/supplemental/10.1103/PhysRevB.107.054435 for the magnetic susceptibility temperature dependence of $KCuPO_4H_2O$ and its deuterated sample are shown.

[26] G. A. Bain, and J. F. Berry, Diamagnetic corrections and Pascal's constants, J. Chem. Educ. **85**, 532 (2008).

[27] J. Sugiyama, Y. Ikedo, M. Månsson, J. H. Brewer, S. L. Stubbs, E. J. Ansaldo, K. H. Chow, J. S. Lord, H. Ohta, C. Michioka, and K. Yoshimura, Magnetic and superconducting nature of

Na$_0$.35CoO$_2 \cdot y$H$_2$O and Na$_0$.35CoO$_2 \cdot y$D$_2$O investigated by muon-spin spectroscopy, Phys. Rev. B **82**, 214505 (2010).

[28] K. Tomiyasu, M. Fujita, A. I. Kolesnikov, R. I. Bewley, M. J. Bull, and S. M. Bennington, Conversion method of powder inelastic scattering data for one-dimensional systems, Appl. Phys. Lett. **94**, 092502 (2009).

[29] M. Fujihala, H. Koorikawa, S. Mitsuda, K. Morita, T. Tohyama, K. Tomiyasu, A. Koda, H. Okabe, S. Itoh, T. Yokoo, S.

Ibuka, M. Tadokoro, M. Itoh, H. Sagayama, R. Kumai, and Y. Murakami, Possible Tomonaga-Luttinger spin liquid state in the spin-$\frac{1}{2}$ inequilateral diamond-chain compound K$_3$Cu$_3$AlO$_2$(SO$_4$)$_4$, Sci. Rep. **7**, 16785 (2017).

[30] M. Karbach, G. Müller, A. H. Bougourzi, A. Fledderjohann, and K.-H. Mütter, Two-spinon dynamic structure factor of the one-dimensional $s = \frac{1}{2}$ Heisenberg antiferromagnet, Phys. Rev. B **55**, 12510 (1997).